

Supplement of Ocean Sci., 15, 809–817, 2019
<https://doi.org/10.5194/os-15-809-2019-supplement>
© Author(s) 2019. This work is distributed under
the Creative Commons Attribution 4.0 License.



Supplement of

Surface predictor of overturning circulation and heat content change in the subpolar North Atlantic

Damien G. Desbruyères et al.

Correspondence to: Damien G. Desbruyères (damien.desbruyeres@ifremer.fr)

The copyright of individual parts of the supplement might differ from the CC BY 4.0 License.

Supplementary information

Statistical analysis

Lagged cross-correlations between variable X and variable Y were performed on annually averaged, low-pass filtered, and detrended time series. The uncertainty of the correlations (given as confidence intervals in the text) were obtained following common practice (McCarthy et al., 2015) that is by

calculating p -values from the t-statistic $T = r \frac{\sqrt{N_{eff} - 2}}{\sqrt{1 - r_{XY}^2}}$ (one-tailed test), where r_{XY} is the correlation and

$N_{eff} = \frac{1 - r_X r_Y}{1 + r_X r_Y}$ is the effective number of degrees of freedom derived from the auto-correlations

r_X and r_Y of the two variables at lag = 1 year (see Table S2).

Lowpass filtered time series presented throughout the paper use a 7-year Hanning window and end-points are therefore truncated at ± 3 years. The impact of low-pass filtering AMOC $_{\sigma}$ and SFOC $_{\sigma}$ time series on the lagged auto-correlations were studied by varying the size of the filtering window (0, 3, 5,

7, 9 and 11 years). While the raw annual time series show small correlations at all lags ($R < 0.4$), maximum correlations for smoothing windows of 3 years and above were reached at a consistent lag of 5-6 years.

Standard errors on linear trends given in the text are obtained from the (rooted) quadratic sum of two error sources: (1) the ensemble standard errors computed as $\frac{\sigma}{\sqrt{N-1}}$, where σ is the standard deviation of the ensemble trends and $N = 4$ the number of data products, and (2) the goodness of the linear fit for the ensemble-mean time series computed as $\sqrt{\frac{\sum r^2}{(n-2)\sum(x-\bar{x})^2}}$, where r are the yearly residuals between the time series and the linear fit, n is the number of years, and x is the time vector.

Supplementary Figures and Tables

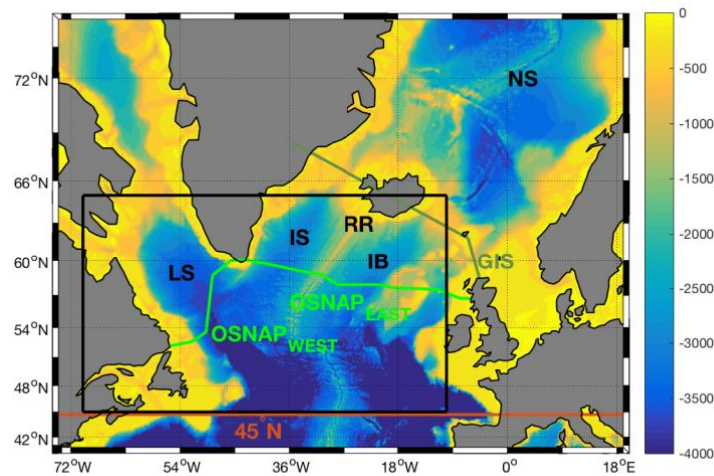


Fig. S1. Study domain with sections discussed in the text: 45°N, GIS (Greenland-Iceland-Scotland sills) and OSNAP. Bathymetric features and basins are highlighted as: Reykjanes Ridge (RR), Iceland Basin (IB), Irminger Sea (IS), Labrador Sea (LS), Nordic Seas (NS). The black box (10°W-70°W; 45°N-65°N) shows the region where the 0-1000m OHC is computed (Figure 3B).

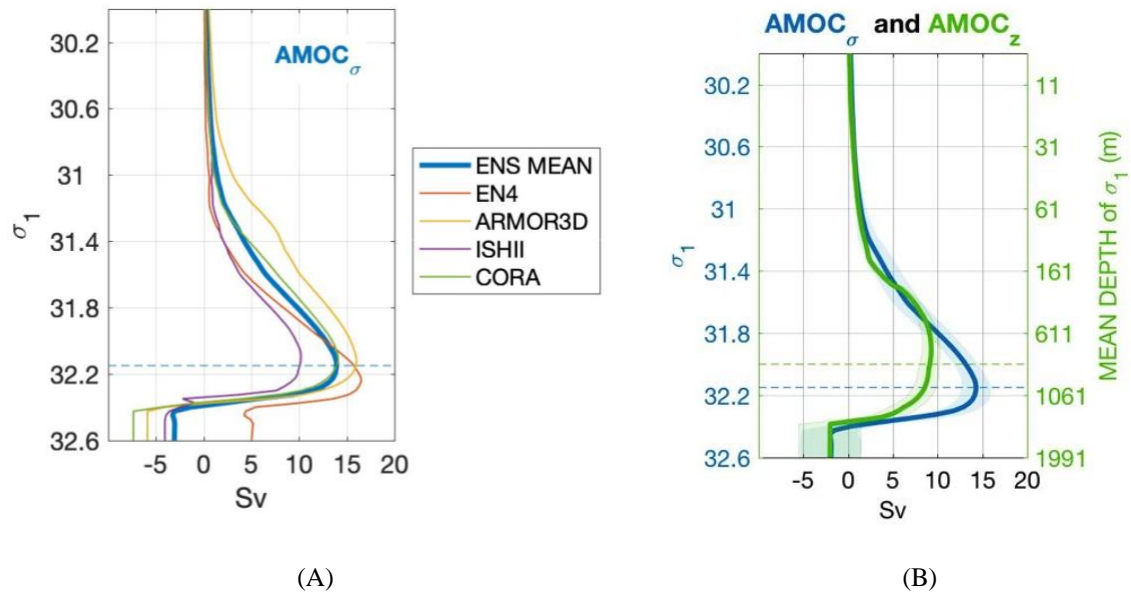
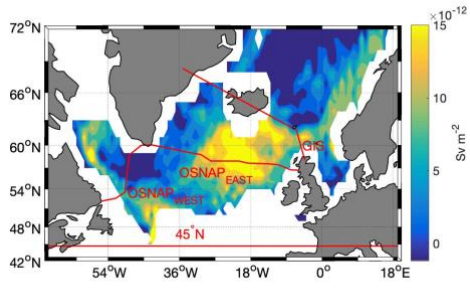
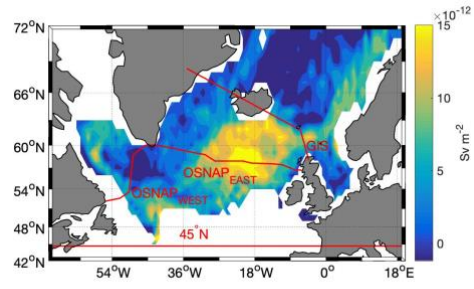


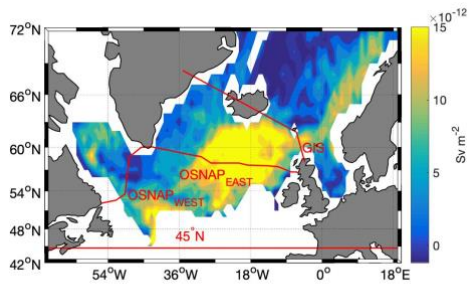
Fig. S2. (A) The time-mean (partial) AMOC $_{\sigma}$ stream function and the associated individual stream function for each product (EN4, ARMOR3D, CORA and ISHII). (B) Comparison of AMOC $_{\sigma}$ (blue) and AMOC $_z$ (green) streamfunction (in Sv), with the latter transposed in density space using the mean depth of σ_1 surfaces at 45°N for easier comparisons (the mean depth of isopycnal is shown on the right-hand y-axis). Shading indicates the ensemble standard error. The blue dashed line at $\sigma_1 = 32.15$ depicts the maximum transformation rate. The green dashed line at 700 m depth depicts the maximum vertical sinking rate.



(A)



(B)



(C)

Fig. S3: The time-mean transformation maps across the isopycnal surface $\sigma_0 = 27.4$ (in Sv m^{-2}) in each of the three reanalysis products used for the ensemble mean of figure 3: (A) NCEP2, (B) ERAI and (C) CERES.

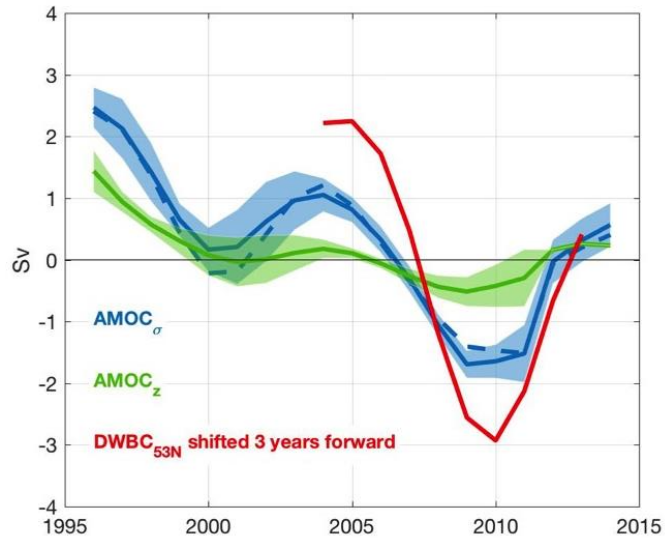


Fig S4. 7-year low pass filtered anomalies in the maximum $AMOC_{\sigma}$ (blue), the maximum velocity-driven $AMOC_{\sigma}$ (blue dashed), and the maximum $AMOC_z$ (green) at $45^{\circ}N$. An independent estimate of the 400m-bottom DWBC intensity at $53^{\circ}N$ is shown in red (shifted 3 years forward). The DWBC data are obtained from 5-day sampled mooring data and converted into annual mean as in column 3, Table 1, in Zantopp et al.: From interannual to decadal: 17 years of boundary current transports at the exit of the Labrador Sea, *Journal of Geophysical Research: Oceans* (2017). DOI: [10.1002/2016JC012271](https://doi.org/10.1002/2016JC012271)".

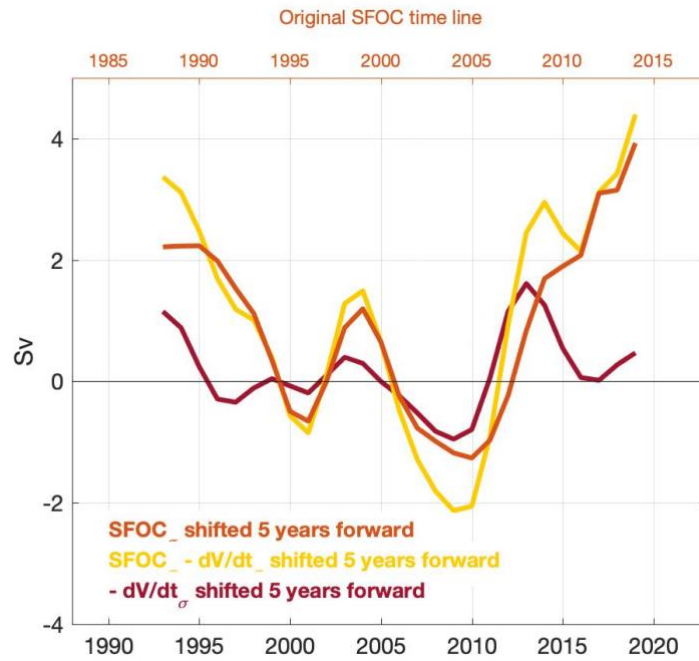


Fig. S5. Verification of the water mass steadiness assumption. The yellow line shows the sum of $SFOC_{\sigma}$ at $45^{\circ}N$ (red) and $-\frac{dV_{\sigma}}{dt}$ the yearly change in the volume of water below the density level of maximum $SFOC_{\sigma}$ (purple). At low-frequency, changes in the surface-forced water transformation rates do not predominantly accumulate as volume anomalies within the SPG but are rather exported within the $AMOC_{\sigma}$ limbs, in good agreement with the $SFOC_{\sigma}/AMOC_{\sigma}$ (delayed) correlation (Figure3A).

	Product	Grid	Period used	Reference
Ocean Analysis	EN4.2.0	1° / 45 levels from 5 to 5350m	1985 – 2017	(Good et al., 2013)
	CORA	0.5° / 152 levels from 0 to 2000 m.	1993 – 2014	10.17882/46219
	ISHII	1° / 24 levels from 0 to 1500m depth	1998 – 2012	(Ishii et al., 2003)
	ARMOR3D	0.25° / 33 levels from 0 to 5500m depth	1993 – 2013	(Guinehut et al., 2012)
Atmospheric Reanalysis	NCEP2	1.875° x 1.915°	1985 – 2017	(Kanamitsu et al., 2002)
	ERA1	0.75°	1985 – 2017	(Dee et al., 2011)
	CERES	0.7°	1985 – 2015	(Liu et al., 2017)

Table S1. The ocean analysis and atmospheric reanalysis used in the present study. Note that CERES does not include freshwater flux variables and is hence combined with NCEP2 to derive the buoyancy fluxes.

X	Y	r	Lag	N_{eff}	T	% (p-value)	Figure
SFOC _{σ} 7-year low passed	AMOC _{σ} 7-year low passed	0.94	5-6	8	6.52	99	3A
$\int MHT_{\sigma}' dt$ (1993-2014)	OHC 0-1000m (1993-2014)	0.87	0	7	3.92	99	3B
$\int MHT_{\sigma}' dt$	OHC 0-1000m	0.50	0	7	1.31	88	3B

Table S2. The statistics of the cross-correlations mentioned in the main text, along with the corresponding Figures where the time series are shown. Positive lags (in years) mean the variable X leads the variable Y (See text for details).

References

- Dee, D. P., Uppala, S. M., Simmons, A. J., Berrisford, P., Poli, P., Kobayashi, S., Andrae, U., Balmaseda, M. A., Balsamo, G., Bauer, P., Bechtold, P., Beljaars, A. C. M., van de Berg, L., Bidlot, J., Bormann, N., Delsol, C., Dragani, R., Fuentes, M., Geer, A. J., Haimberger, L., Healy, S. B., Hersbach, H., Hólm, E. V., Isaksen, I., Kållberg, P., Köhler, M., Matricardi, M., McNally, A. P., Monge-Sanz, B. M., Morcrette, J. J., Park, B. K., Peubey, C., de Rosnay, P., Tavolato, C., Thépaut, J. N. and Vitart, F.: The ERA-Interim reanalysis: Configuration and performance of the data assimilation system, *Q. J. R. Meteorol. Soc.*, 137(656), 553–597, doi:10.1002/qj.828, 2011.
- Good, S. A., Martin, M. J. and Rayner, N. A.: EN4: Quality controlled ocean temperature and salinity profiles and monthly objective analyses with uncertainty estimates, *J. Geophys. Res. Ocean.*, 118(12), 6704–6716, doi:10.1002/2013JC009067, 2013.
- Guinehut, S., Dhomps, A.-L., Larnicol, G. and Le Traon, P.-Y.: High resolution 3-D temperature and salinity fields derived from in situ and satellite observations, *Ocean Sci.*, 8(5), 845–857, doi:10.5194/os-8-845-2012, 2012.
- Ishii, M., Kimoto, M. and Kachi, M.: Historical Ocean Subsurface Temperature Analysis with Error Estimates, *Mon. Weather Rev.*, 131(1), 51–73, doi:10.1175/1520-0493(2003)131<0051:HOSTAW>2.0.CO;2, 2003.
- Kanamitsu, M., Ebisuzaki, W., Woollen, J., Yang, S.-K., Hnilo, J. J., Fiorino, M. and Potter, G. L.: Ncep--doe amip-ii reanalysis (r-2), *Bull. Am. Meteorol. Soc.*, 83(11), 1631–1643, doi:10.1175/BAMS-83-11, 2002.
- Liu, C., Allan, R. P., Mayer, M., Hyder, P., Loeb, N. G., Roberts, C. D., Valdivieso, M., Edwards, J. M. and Vidale, P. L.: Evaluation of satellite and reanalysis-based global net surface energy flux and uncertainty estimates, *J. Geophys. Res.*, 122(12), 6250–6272, doi:10.1002/2017JD026616, 2017.
- McCarthy, G. D., Haigh, I. D., Hirschi, J. J.-M., Grist, J. P. and Smeed, D. A.: Ocean impact on decadal Atlantic climate variability revealed by sea-level observations, *Nature*, 521(7553), 508–510, doi:10.1038/nature14491, 2015.